


Efficient entanglement between two long-distance quantum emitters mediated by dark-gap-plasmon waveguides

Hua Qiu, Yue You, Xi-Hua Guan, Xiao-Jing Du, Jun He , and Zhong-Jian Yang ^{*}

Hunan Key Laboratory of Nanophotonics and Devices, School of Physics, Central South University, Changsha 410083, China



(Received 4 June 2024; revised 21 July 2024; accepted 19 August 2024; published 29 August 2024)

We theoretically investigate the entanglement between two well-separated quantum emitters (QEs) mediated by dark-gap-plasmon waveguides. Both the plasmon-QE coupling strength and the energy transfer efficiency between QEs are crucial for entanglement based on analytical results. To overcome the low energy transfer efficiency brought by common plasmonic waveguides, we construct a simple dark-gap-plasmon waveguide. Such a structure consists of two parallel silver nanowires, where dark plasmon modes are formed in the gap between the two nanowires. The leaky (or radiative) feature of propagating plasmons is highly suppressed, which results in the quality factors of the dark plasmon modes reaching the material limit. Thus, the energy transfer efficiency can reach more than 94% with a distance even over ten working wavelengths ($> 10 \mu\text{m}$). Meanwhile, by introducing a tip dimer structure in the nanowire gap, the plasmon-QE coupling can reach a strong coupling regime with realistic parameters. The influences from the geometric parameters of the system are also considered. The energy transfer efficiency is robust to the geometric variations due to the dark feature of the plasmon responses.

DOI: [10.1103/PhysRevB.110.075432](https://doi.org/10.1103/PhysRevB.110.075432)

I. INTRODUCTION

Controlling the interactions between photons and quantum emitters (QEs) such as molecules or quantum dots is important for many applications including quantum information, nanolasers, and chemical reactions [1–5]. Among the photonic structures, plasmonic nanostructures have become an attractive platform to achieve desirable couplings with QEs, especially at room temperature [6–12]. This is due to the well-known high near-field concentration ability accompanied by surface plasmon resonances [13]. The coupling strength between a plasmon mode and a single QE is a fundamental parameter that has attracted many researchers. Besides involving a QE with a large enough transition dipole moment, one efficient way is to squeeze the mode volume of a plasmonic nanostructure. This is usually achieved by introducing a small gap between plasmonic structures [6–8]. In recent years, significant progress has been made in achieving larger plasmon-QE coupling strengths. The coupling strength between the plasmon modes and a single QE can now reach the strong coupling regime at room temperature [6–9, 14–17], which means the energy can transfer back and forth between the plasmons and a QE.

Achieving efficient entanglement between two QEs represents an important step towards quantum control of QEs and is crucial for applications such as quantum information [18–22]. Short-distance entanglement can be achieved through a single optical cavity that mediates two QEs [23–30], where the plasmon-QE coupling strength plays a key role in the entanglement amplitude. Despite these theoretical

advancements, there have been almost no experimental reports of entanglement between two QEs mediated by plasmonic nanostructures. The main reason could lie in the fact that the QEs are spatially too close to each other experimentally. One experimentally feasible way is to establish efficient entanglement between two distanced QEs so that the excitation and measurement can be carried out at well-separated locations [23]. More importantly, the entanglement between two qubits with a long enough distance may also be necessary for the application of quantum information [31–41]. In fact, efforts have been devoted to theoretically studying the entanglement between two distanced QEs mediated by plasmonic nanostructures including wedge waveguides, and single nanowires [42–49]. In such systems, in addition to the plasmon-QE coupling strength, another typical important parameter is the energy transfer efficiency between two QEs. The limited energy transfer efficiency is a disadvantage factor for entanglement, and it is usually induced by the material loss and radiative loss of a plasmon resonance. Thus, the energy transfer efficiencies in the proposed strategies reduce quickly with distance and remain less than ~ 0.9 after propagating only one or two working wavelengths [49]. Furthermore, the coupling strengths in those systems are relatively lower than those with subwavelength plasmonic cavities. A tricky issue is that by narrowing the gaps between QEs and plasmonic structures, the plasmon-QE coupling strength could be increased while the energy transfer efficiency would usually drop even further [49, 50].

In this study, we construct dark-gap-plasmon modes within plasmonic nanostructures to facilitate quantum entanglement between two distanced QEs. Our approach utilizes two parallel silver (Ag) nanowires to generate dark plasmon modes within their gap. Correspondingly, the leaky (or radiative)

^{*}Contact author: zjyang@csu.edu.cn

feature of propagating plasmon is highly suppressed in such a system and the quality (Q) factor of the dark plasmon modes is almost purely determined by the material loss. Remarkably, the energy transfer efficiency can be maintained over 94% even when the QEs are separated by a distance exceeding ten working wavelengths ($> 10 \mu\text{m}$). More calculations show that the energy transfer efficiency is almost only affected by the material loss and is robust to the geometric variations due to the dark feature of the plasmon responses. Furthermore, by introducing a tip dimer around the QE in the dark-gap-plasmon waveguide, the plasmon-QE coupling strength can reach a strong regime with realistic parameters. We also consider the effects of geometric parameters on the entanglement within this system.

II. THEORETICAL METHODS

The dynamic evolution of QEs coupled to a lossy plasmon nanostructure can be characterized in the form of a well-known quantum master equation

$$\frac{\partial \hat{\rho}}{\partial t} = \frac{1}{i\hbar} [\hat{H}, \hat{\rho}] + L(\hat{\rho}), \quad (1)$$

where $\hat{\rho}$ is the density matrix describing the state of the system, \hat{H} is the Hamiltonian of the system, and the Lindblad superoperator L can be used to describe the loss in the system. In the model involving the entanglement of two QEs mediated by a plasmonic waveguide, each QE is a two-level system, namely, a ground state $|g\rangle$ and an excited state $|e\rangle$. The number of photons in the plasmon waveguide can be represented by s . The wave function representing the state of the system can be expressed as $|\Psi(t)\rangle = |q_1\rangle |q_2\rangle |s\rangle$, where $q_i = e$ or g , and the number of photons $s = 0, 1, 2 \dots s_{\text{max}}$. Then, the density matrix ρ can be expressed as [23]

$$\begin{aligned} \hat{\rho}(t) &= |\Psi(t)\rangle \langle \Psi(t)| \\ &= \sum_{q_1, q_2, s, q_1^*, q_2^*, s^*} |q_1\rangle |q_2\rangle |s\rangle \langle q_1^*| \langle q_2^*| \langle s^*|, \end{aligned} \quad (2)$$

Under the rotational wave approximation, the Hamiltonian H of the system can be expressed as [51,52]

$$\hat{H} = \sum_{i=1,2} \hbar\omega_0 \hat{\sigma}_i^\dagger \hat{\sigma}_i + \hbar\omega_c \hat{b}^\dagger \hat{b} + \hbar \sum_{i=1,2} g_i \beta^{2g_i} (\hat{\sigma}_i^\dagger \hat{b} + \hat{\sigma}_i \hat{b}^\dagger), \quad (3)$$

where ω_0 denotes the dipole transition frequency of a QE and ω_c denotes the resonance frequency of the plasmon mode. It is assumed that the QEs are in resonance with the plasmon mode ($\omega_0 = \omega_c$). $\hat{\sigma}_i^\dagger$ ($\hat{\sigma}_i$) represents the raising (lowering) operator of the i th QE, \hat{b}^\dagger (\hat{b}) represents the generation (annihilation) operator of a plasmon, g_i represents the coupling strength between the i th QE and the waveguide, and β represents the energy transfer efficiency between the two QEs. β is included due to the fact that the energy can transfer between the QEs through a waveguide; the proportion of energy returned to a QE in each round (g_i) is β^2 . The Lindblad superoperator describes the plasmon loss, QE spontaneous radiation loss, and dephase caused by the external environment. Thus, it can be given by the following equation

[11,53]:

$$\begin{aligned} L &= \frac{\gamma_s}{2} (2\hat{b}\hat{\rho}\hat{b}^\dagger - \hat{b}^\dagger\hat{b}\hat{\rho} - \hat{\rho}\hat{b}^\dagger\hat{b}) \\ &+ \sum_{i=1,2} \frac{\gamma_0}{2} (2\hat{\sigma}_i\hat{\rho}\hat{\sigma}_i^\dagger - \hat{\sigma}_i^\dagger\hat{\sigma}_i\hat{\rho} - \hat{\rho}\hat{\sigma}_i^\dagger\hat{\sigma}_i) \\ &+ \sum_{i=1,2} \gamma_d (2\hat{\sigma}_i^\dagger\hat{\sigma}_i\hat{\rho}\hat{\sigma}_i^\dagger\hat{\sigma}_i - \hat{\sigma}_i^\dagger\hat{\sigma}_i\hat{\rho} - \hat{\rho}\hat{\sigma}_i^\dagger\hat{\sigma}_i), \end{aligned} \quad (4)$$

where γ_s represents the decay rate of a plasmon mode, γ_0 represents the decay rate of an individual QE in vacuum, and γ_d represents environmental dephasing decay constant.

By solving the master equation, Eq. (1), one can obtain the density matrix $\hat{\rho}(t)$ as a function of time. As for the entanglement between QEs, it is necessary to reduce the photon number states in the plasmon waveguide (details of the derivation can be found in the Supplemental Material [54]), and the reduced density matrix for the states of two QEs can be written as

$$\hat{\rho}_{12}(t) = \sum_{s=0,1} \langle s | \hat{\rho}(t) | s^* \rangle. \quad (5)$$

The entanglement between two QEs is measured by the degree of concurrence [55], which can be obtained by the reduced density matrix $\hat{\rho}_{12}(t)$,

$$C(\hat{\rho}_{12}(t)) = \max\{0, \lambda_1 - \lambda_2 - \lambda_3 - \lambda_4\}, \quad (6)$$

where $\lambda_1, \lambda_2, \lambda_3, \lambda_4$ are the square roots of the four eigenvalues of the matrix $\hat{\rho}_{12}(t)\hat{\tilde{\rho}}_{12}(t)$ in descending order, where $\hat{\tilde{\rho}}_{12}(t)$ is the spin-flipped state of $\hat{\rho}_{12}(t)$ (see details in the Supplemental Material [54]).

The plasmon-QE coupling strength g_i and the energy transfer efficiency β are greatly dependent on the properties of plasmonic waveguides which are highly tunable. The contributions from an electromagnetic mode in a plasmon waveguide to the spectral density can be expressed as $|g(\omega_0)|^2 = \frac{\omega_0^2}{\hbar\pi\epsilon_0c^2} \text{Im}[\boldsymbol{\mu}_i^* \mathbf{G}(\mathbf{r}_i, \mathbf{r}_i, \omega_0) \boldsymbol{\mu}_i]$, where $\boldsymbol{\mu}_i$ denotes the electric dipole moment of QE $_i$, and the Green's function $\mathbf{G}(\mathbf{r}_i, \mathbf{r}_j, \omega_0)$ describes the dipole interaction between QEs. The coupling strength can be approximated by a Lorentzian near a resonance [56] $|g(\omega_0)|^2 = \frac{g_i^2}{2\pi} \frac{\gamma_s}{(\omega_0 - \omega_c)^2 + (\frac{\gamma_s}{2})^2}$. Here, \hbar is the reduced Planck constant, c is the speed of light, and ϵ_0 is the dielectric constant in a vacuum. So, the resonant g_i can be expressed in terms of the Green's function as $\frac{4g_i^2}{\gamma_s} = \frac{2\omega_0^2}{\hbar\epsilon_0c^2} \text{Im}[\boldsymbol{\mu}_i^* \mathbf{G}(\mathbf{r}_i, \mathbf{r}_i, \omega_0) \boldsymbol{\mu}_i]$. For a general plasmonic structure, the Green's function cannot be solved analytically. On the other hand, the Green's function can be numerically obtained based on the electric field $\mathbf{E}(\mathbf{r}_i)$ generated at the \mathbf{r}_i by a dipole light source located in the \mathbf{r}_j . For example, the electric field can be simulated by the finite time-domain difference method (FDTD; see more details in the Supplemental Material [54]), and then the Green's function $\mathbf{G}(\mathbf{r}_i, \mathbf{r}_j)$ can be obtained based on [49]

$$\mathbf{E}(\mathbf{r}_i, \omega_0) = \omega_0^2 \mu_0 \mathbf{G}(\mathbf{r}_i, \mathbf{r}_j, \omega_0) \boldsymbol{\mu}_j, \quad (7)$$

where μ_0 is the vacuum permeability and $\boldsymbol{\mu}_j$ is the electric dipole moment of the QE $_j$.

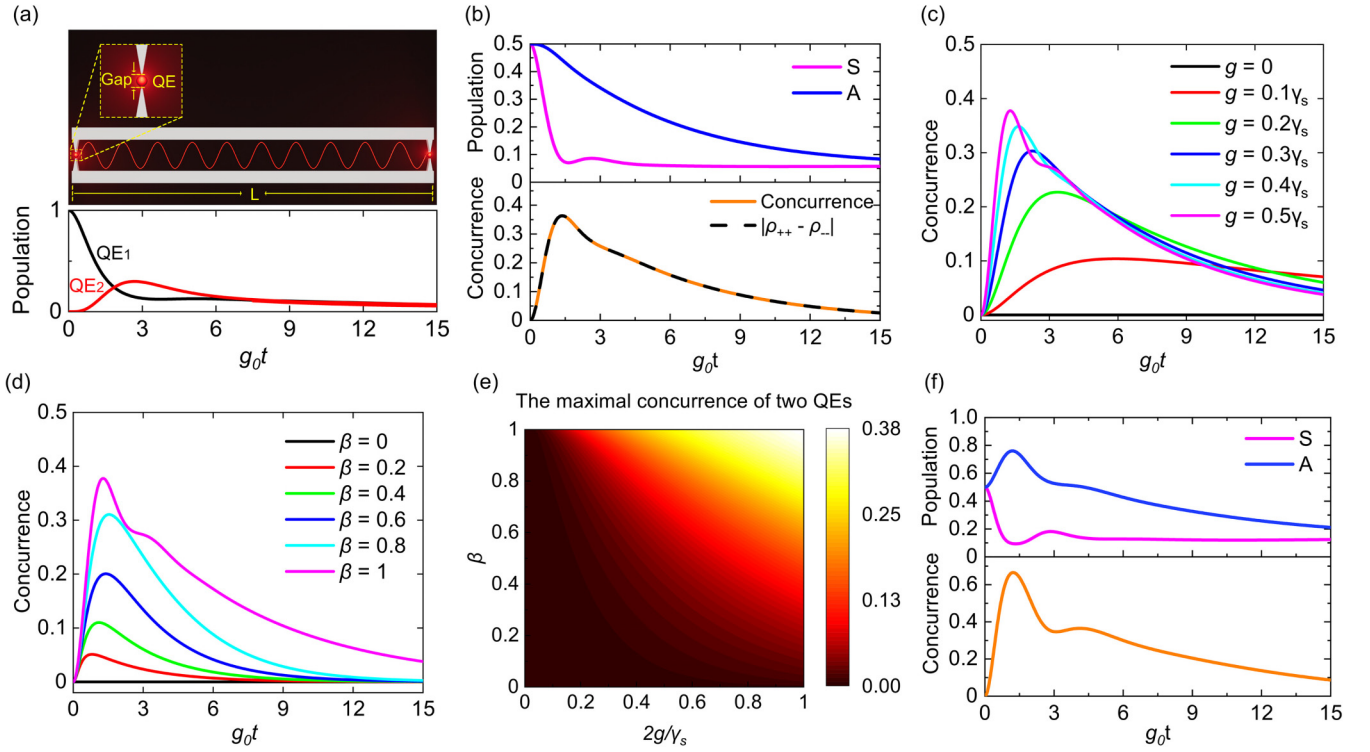


FIG. 1. (a) Top: schematic of a Ag nanowire waveguide structure with two QEs. Bottom: the evolution of the excited state population of QEs over time. Here, we assume a given loss γ_s ($= 2g_0$) for a plasmonic system and the QE-plasmon coupling strength $g=g_0$. $g_1=g_2$ and β is taken to be $\beta = 0.95$. (b) Top: populations of the Bell states S and A in the above two QEs systems. Bottom: the evolution of concurrence in two QE systems over time. (c) Effects of coupling strength g on concurrence evolution, $\beta = 1$, $g_1=g_2=g$. (d) Effect of β factor on concurrence evolution, $g_1=g_2=g_0$. (e) The peak value of concurrence as a function of g and β , $g_1=g_2=g$. (f) Top: populations of the Bell states S and A in a two QE system under the condition of $\frac{g_2}{g_1} = \frac{1}{\sqrt{2}-1}$. Bottom: the evolution of concurrence in two QEs systems over time. $g_1=g_0$. For all figures, we have $\gamma_d = 0.1\gamma_s$ and $\gamma_0 = 10^{-4}\gamma_s$.

The energy transfer efficiency β is obtained based on the decay rate enhancements of the QEs in the plasmonic waveguide structure. The decay rate enhancements of the QEs can also be calculated based on the Green's function. The decay rate γ_{ii} of QE $_j$ due to self-interaction in a plasmon waveguide is also known as the spontaneous radiation rate $\gamma = \frac{4g_i^2}{\gamma_s}$. The decay rate γ_{ij} due to the interaction between QEs can be expressed as [48,55–57]

$$\gamma_{ij} = \frac{2\omega_0^2}{\hbar\epsilon_0 c^2} \text{Im}[\boldsymbol{\mu}_i^* \mathbf{G}(\mathbf{r}_i, \mathbf{r}_j, \omega_0) \boldsymbol{\mu}_j]. \quad (8)$$

The energy transfer efficiency β represents the ratio of γ_{ij} to γ_{ii} :

$$\beta = \frac{\gamma_{ij}}{\gamma_{ii}} = \frac{\text{Im}[\boldsymbol{\mu}_i^* \mathbf{G}(\mathbf{r}_i, \mathbf{r}_j, \omega_0) \boldsymbol{\mu}_j]}{\text{Im}[\boldsymbol{\mu}_i^* \mathbf{G}(\mathbf{r}_i, \mathbf{r}_i, \omega_0) \boldsymbol{\mu}_i]}. \quad (9)$$

By combining the simulation results from FDTD with Eq. (7), one can obtain the coupling strength g_i and energy transfer efficiency β . Alternatively, g_i can also be obtained by the Purcell factor F , which represents the enhancement of the spontaneous radiation of QE. It can be expressed in terms of the Green's function as [48,58]

$$F = \frac{\gamma}{\gamma_0} = \frac{6\pi c}{\omega_0} \text{Im}[\boldsymbol{\mu}_i^* \mathbf{G}(\mathbf{r}_i, \mathbf{r}_i, \omega_0) \boldsymbol{\mu}_i]. \quad (10)$$

The spontaneous emission rate of a QE in vacuum is given by $\gamma_0 = \frac{\omega_0^3 |\boldsymbol{\mu}_e|^2}{3\pi\epsilon_0 \hbar c^3}$, where $\boldsymbol{\mu}_e$ is the transition dipole moment. According to Fermi's golden rule, at the weak coupling limit, F can be expressed as a function of g_i as [23,59]

$$F = \frac{4g_i^2}{\gamma_s \gamma_0}. \quad (11)$$

For a general plasmonic structure, F can be easily simulated by the FDTD directly. It should be noted that although Eq. (10) only holds with a weak coupling strength, the Green's function itself remains the same with different $\boldsymbol{\mu}_i$. In the FDTD simulations, the $\boldsymbol{\mu}_i$ is always small enough to ensure the validity of Eq. (10). Thus, Eq. (11) can be safely used for the calculation of g_i even under the strong coupling condition, as Eq. (10) is just used to obtain the Green's function for g_i . One needs to recognize that if a system is in the strong coupling regime, Eq. (10) cannot be used for the calculation of the Purcell factor anymore, as this concept does not hold in this situation.

III. RESULTS

To specifically reveal the impacts of the plasmon-QE coupling strength g and the energy transfer efficiency β on the entanglement, we analytically consider two identical two-level QEs placed within a general plasmonic waveguide structure [Fig. 1(a)]. The initial state of the system is

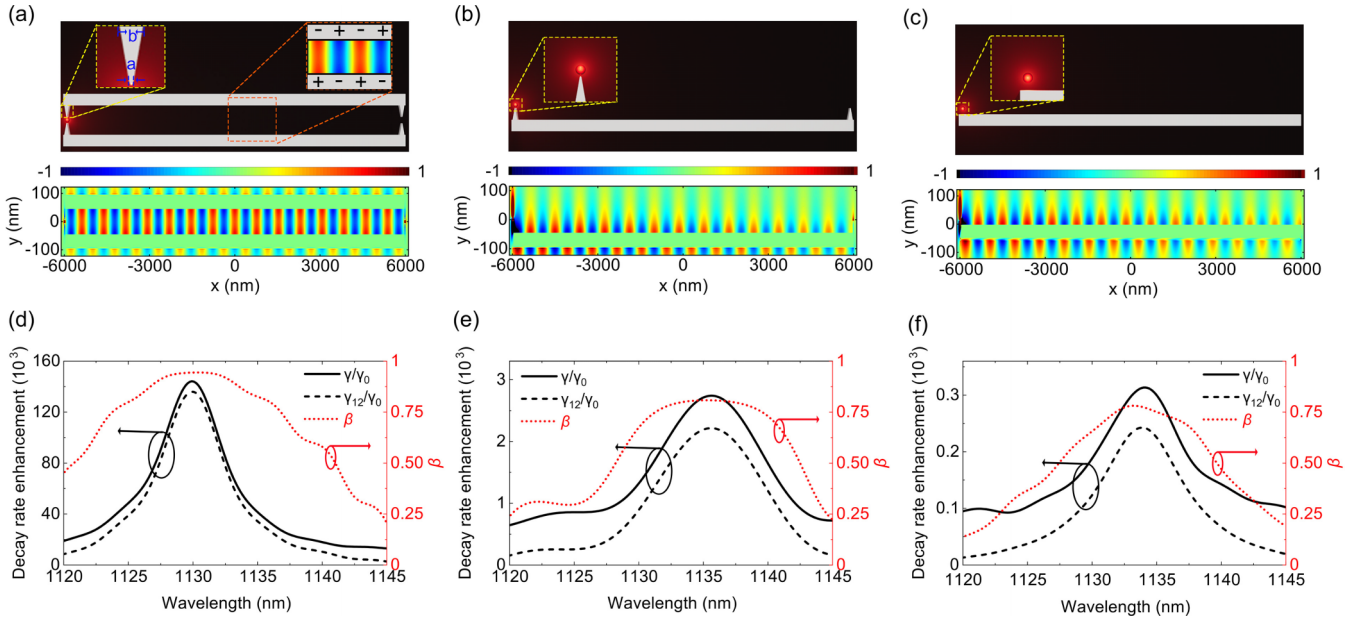


FIG. 2. The decay rate enhancement and energy transfer efficiency β with different waveguides. The length, width, and height of a nanowire for each configuration are $12 \mu\text{m}$, 50 nm , and 50 nm , respectively. (a) Top: the schematic of a dark-gap-plasmon waveguide and the charge distributions. The separation between the two nanowires is 90 nm . The length b for a triangle is $b = 10 \text{ nm}$ and the tip is rounded with a disk of diameter $a = 1 \text{ nm}$. Bottom: the distribution of the imaginary part of the normalized electric field $\text{Im}[E_y]$ in the waveguide at the resonant wavelength $\lambda = 1130 \text{ nm}$. (b) A single wire waveguide and the resonant field distribution of normalized $\text{Im}[E_y]$ at $\lambda = 1135 \text{ nm}$. (c) The same content as (b) while the tip is removed. In all configurations, the QE-metal distance is the same (2 nm) for the sake of comparison. The decay rate enhancements γ/γ_0 (γ_{11}/γ_0), γ_{12}/γ_0 and the energy transfer efficiency β corresponding to the structures in (a), (b), and (c) are shown in (d), (e), and (f), respectively.

assumed to be that QE_1 is in the excited state $|e\rangle$, QE_2 is in the ground state $|g\rangle$, and the number of photons in the plasmon waveguide is 0, namely, $|\Psi(0)\rangle = |e\rangle|g\rangle|0\rangle$. In this case, the energy emitted by QE_1 can be transferred to QE_2 via the waveguide. Figure 1(a) also shows the dynamics of a typical system based on the quantum electrodynamics [51] as described by Eq. (1). The QEs exchange energy without interruption and transition between the ground state and the excited state. The population of the two QEs on the Bell states can help us better understand the dynamics of entanglement. The concurrence can be expressed as $C(t) = \sqrt{(\rho_{++} - \rho_{--})^2 + 4\text{Im}(\rho_{+-})^2}$, where ρ_{++} is the population of the Bell state $S = \frac{1}{\sqrt{2}}(|10\rangle + |01\rangle)$ and ρ_{--} is the population of the Bell state $A = \frac{1}{\sqrt{2}}(|10\rangle - |01\rangle)$. When the initial state of the system is $|\Psi(0)\rangle = |e\rangle|g\rangle|0\rangle$, $\text{Im}(\rho_{+-}) \equiv 0$. Then, $C(t)$ can be simplified as $C(t) = \sqrt{(\rho_{++} - \rho_{--})^2} = |\rho_{++} - \rho_{--}|$ [Fig. 1(b)]. Therefore, the Bell state can also well reflect the degree of entanglement between QEs.

Figures 1(c) and 1(d) show the effects of the coupling strength g_i and the energy transfer efficiency β on the concurrence between QEs. Here, we have assumed the coupling strength between QE_1 and a waveguide (g_1) is the same as that between QE_2 and the waveguide (g_2), namely, $g_1 = g_2 = g$. At the same time, it can still reflect the main feature of the influence of coupling strength g on the entanglement. g and β can both significantly affect the entanglement behaviors of the two QEs. The maximal entanglement as a function of g and β is shown in Fig. 1(e), where the coupling strength g is varied in a realistic range based on current plasmonic

systems, namely, $2g/\gamma_s \sim 1$ [17]. More calculations show that the maximal entanglement can be further increased by further increasing the coupling strengths and making the coupling strengths g_1 and g_2 different. For the most common initial state of the system $|\Psi(0)\rangle = |e\rangle|g\rangle|0\rangle$, the entanglement between QEs can be optimized by setting $\frac{g_2}{g_1} = \frac{1}{\sqrt{2}-1}$ (see Fig. S1 in the Supplemental Material [54]). The concurrence value will become relatively almost twice larger than the situation with $g_1 = g_2$ [Figs. 1(b) and 1(f)]. As mentioned earlier, the coupling strength g and energy transfer efficiency β are highly dependent on the properties of the plasmonic waveguide. On the other hand, in most plasmonic waveguides the optimizations of g and β are usually in conflict with each other [49,50]. In the following part of this paper, we will take the assumption $g_1 = g_2 = g$ as a default condition for simplicity. We note that the concurrence under this condition will be obviously smaller than 1, while this value can be easily increased by tuning the ratio of g_1 and g_2 .

Here, we construct a simple plasmon waveguide composed of two parallel Ag nanowires [Fig. 2(a)]. The Ag nanowires are separated by a certain distance and a tip dimer structure is designed at the location of each QE to enhance the couplings between QEs and the waveguide. Here, choosing the geometric parameters highly relies on their influences on the g and β , which will be discussed in detail later. In such a structure, the charges are opposite on the two sides of the gap, and a dark-gap-plasmon resonance is formed in the gap at $\lambda = 1130 \text{ nm}$ [Figs. 2(a) and 2(d)]. Correspondingly, the plasmon energy is well confined between the two nanowires [Fig. 2(a)], which can efficiently suppress the transmission loss and results in a

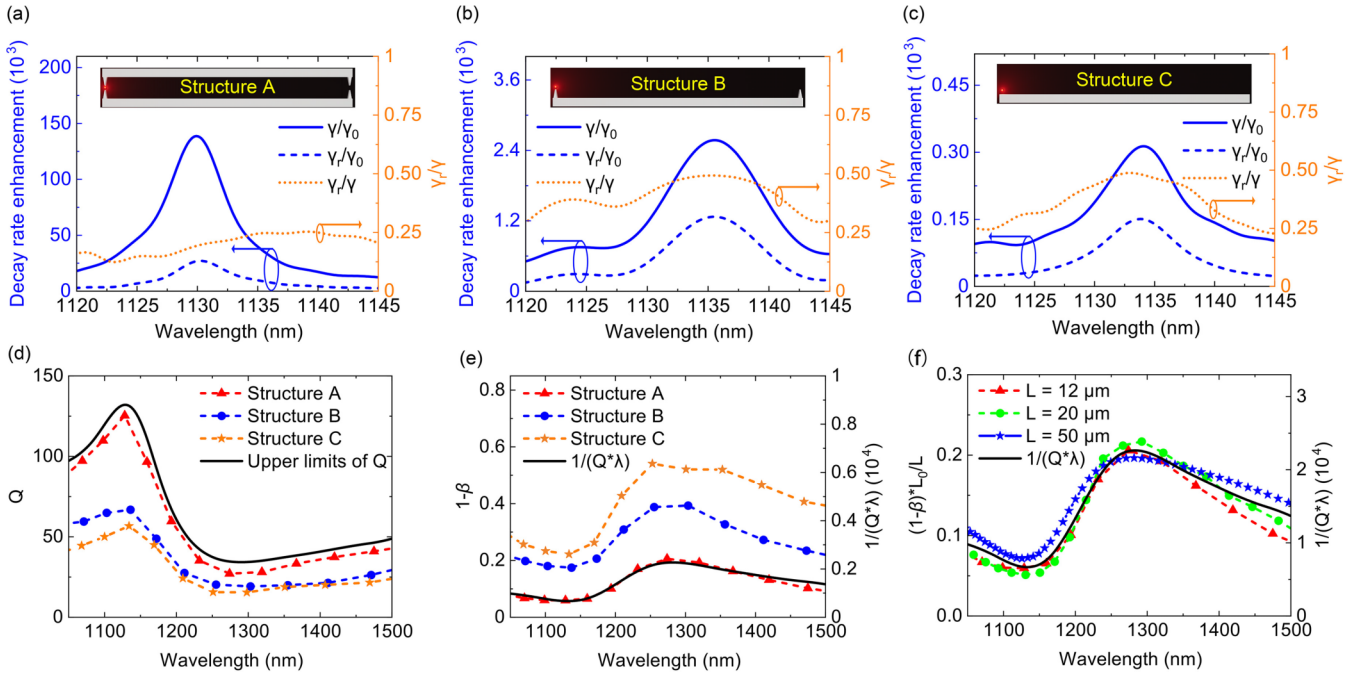


FIG. 3. (a) The total (γ/γ_0) and radiative (γ_r/γ_0) decay rate enhancement for the dark-gap-plasmon waveguide (structure A). The ratio of γ_r/γ is also shown. The results for single wire waveguides of structures B and C are shown in (b) and (c), respectively. The structures A, B, and C are the same as those in Fig. 2. (d) Q factors as a function of working wavelength corresponding to plasmon modes in the three different waveguides and the theoretical prediction of maximum values of Q determined by material properties. (e) The relation between the $1/(Q\lambda)$ and $1-\beta$ corresponding to each plasmon mode in three different Ag waveguides. (f) The relation between the $1/(Q\lambda)$ and normalized $1-\beta$ corresponding to each plasmon mode in the dark-gap-plasmon waveguide with different lengths, where L_0 is taken as $L_0 = 12 \mu\text{m}$.

high energy transfer efficiency of 94.1% with a long distance of 12 μm [Fig. 2(d)]. This length is more than ten working wavelengths. Furthermore, the coupling strength g can be greatly enhanced by introducing the tip dimer surrounding the QEs. Here it can be verified based on Eq. (11) that g is larger than $\gamma_s/2$ indicating a strong coupling regime under this situation [17,52]. This is due to the fact that the gap formed by the two small triangular structures can localize the electromagnetic field energy in a small area, which can enhance the coupling between the QE and the plasmon. On a whole, both a large coupling strength and a high energy transfer rate can be obtained.

In contrast to the above configuration, if the tip structure is broken or removed, the decay rate enhancement drops almost one order of magnitude [Figs. 2(d)–2(f)]. Furthermore, as the dark-gap-plasmon configuration is broken, the energy transfer efficiency β also decreases significantly [Figs. 2(d)–2(f)]. The leaky feature of the propagating plasmon in a single nanowire without the dark-gap-plasmon feature is also obviously demonstrated by the near-field distributions [Figs. 2(b) and 2(c)]. The energy transfer efficiency β of the two parallel wires waveguide without the sharp tips is only around 65% (see Fig. S2 in the Supplemental Material), which is even significantly lower than the cases in Fig. 2(c).

Due to the formation of dark gap plasmons, the radiative losses can be greatly suppressed during the plasmon energy transfer between QEs. This is directly confirmed by the simulations as shown in Figs. 3(a)–3(c). The ratio of radiative decay rate to the total decay rate of a QE drops from $\sim 50\%$ for a single nanowire to less than 20% for the dark-gap-plasmon

waveguide at the working wavelength corresponding to a plasmon resonance. This value is close to the baseline which could be caused by the tails of other modes. As the radiative decay channel is largely suppressed, the plasmon energy transfer factor β should be dominated by the loss of the material itself. This is also confirmed by the numerical calculations.

It is known that in metal nanostructures, when the radiative loss is negligible, the quality factor Q of a plasmon mode can be expressed as [60]

$$Q = \frac{\omega \frac{d\varepsilon'_m}{d\omega}}{2\varepsilon''_m}, \quad (12)$$

where ε'_m (ε''_m) is the real (imaginary) part of the dielectric function of a metal. The Q factor can also be expressed as [60] $Q = \frac{\omega}{2\Delta\omega} = \frac{\omega}{2\gamma_s}$. One finds that the Q factor of the dark plasmon mode is close to that determined by the material limit [Figs. 3(d) and S2]. On the other hand, if the radiative loss takes an increasing role for the loss of a plasmon mode, the Q factor will drop obviously as illustrated by the cases with single wire waveguides [Figs. 3(d) and S3].

In a plasmon mode, if the energy decay is only determined by the material loss, the relation between γ_s and β should satisfy $\gamma_s \propto 1-\beta$. Then, one finds

$$\frac{1}{1-\beta} \propto \frac{1}{\gamma_s} = \frac{Q\lambda}{\pi c}, \quad (13)$$

namely,

$$1-\beta \propto \frac{1}{Q\lambda}. \quad (14)$$

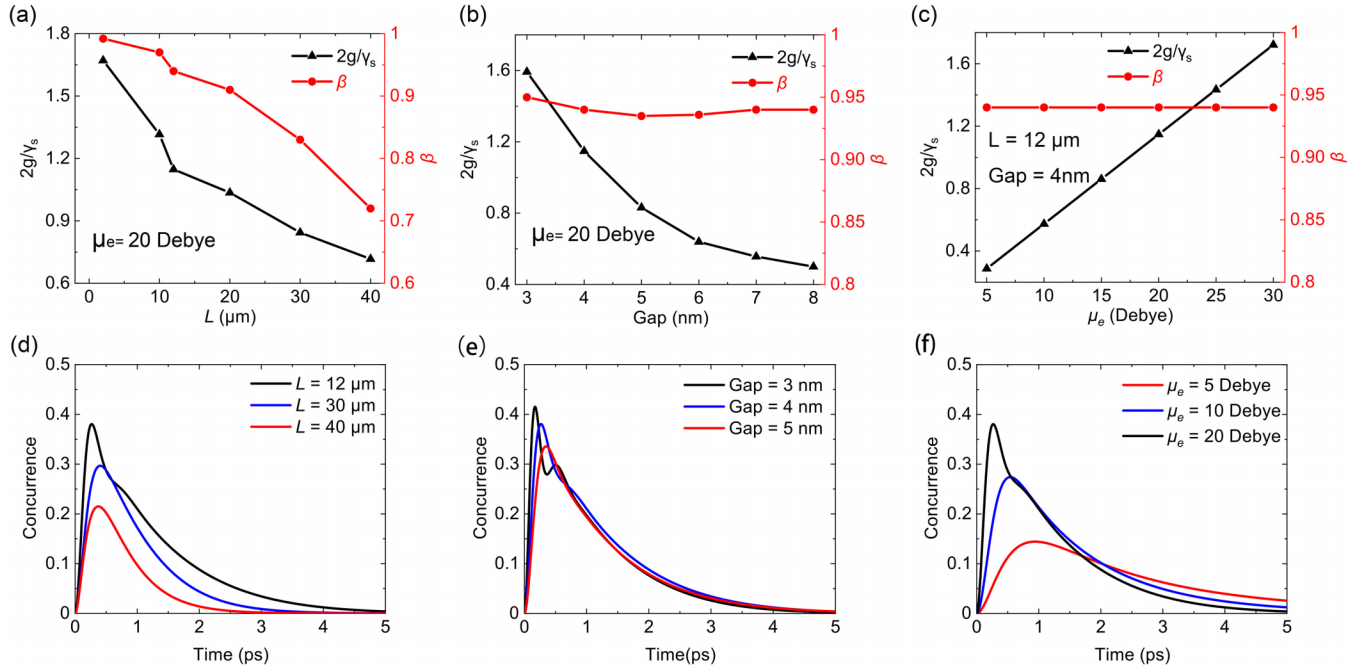


FIG. 4. The energy transfer efficiency β and the coupling strength g with different lengths (a), gaps of the tip dimer (b), and the transition dipole moment of each QE (c). In each figure, the other parameters of the dark-gap-plasmon waveguide are the same as that in Fig. 2(a). The transition dipole moment of each QE is 20 D in (a) and (b). The concurrence of QEs as a function of time corresponding to different cases in (a), (b), and (c) are shown in (d), (e), and (f), respectively.

Figure 3(e) shows the results of the $1-\beta$ and $1/(Q\lambda)$ as a function of wavelength for a dark-gap-plasmon waveguide. Here, the results of $1-\beta$ are directly simulated by the FDTD and that of $1/(Q\lambda)$ are calculated based on the Ag material properties [Eq. (12)]. They agree well and verify the validity of Eq. (14) in such a dark-gap-plasmon system. In contrast, as the resonant radiative decay takes an important role in the plasmon transmission loss for a single wire waveguide, the energy transfer efficiency β does not follow the trend of material loss well [Fig. 3(e)]. Figure 3(f) shows the relationship between the $1-\beta$ and $1/(Q\lambda)$ of dark-gap-plasmon waveguides with different lengths. They all follow the trend of material loss well due to the highly suppressed radiative decay rate enhancements near resonances. Since the transfer efficiency β is highly determined by the material loss, it can also be verified that if the Ag is replaced by another common material, gold (Au), the β will drop obviously due to the higher material loss of Au (see Fig. S4).

The energy transfer efficiency β and the coupling strength g can be affected by the geometries of the plasmon waveguide and the transition dipole moment of a QE. Figure 4(a) illustrates that the energy transfer efficiency β can reach 99.2% when the distance between QEs is about $2 \mu\text{m}$ (~ 1.7 times the working wavelength). β remains 94.1% when the distance is increased to $12 \mu\text{m}$, which ensures that the energy between QEs can be efficiently transmitted through the waveguide. The increase in the waveguide length will also lead to a decrease in the coupling strength g between the QE and the waveguide. This is closely related to the fact that the light concentration ability usually decreases with relatively increased volume [17,61]. As expected, the ability to concentrate the electromagnetic field decreases by increasing

the gap between two triangle tips, and the coupling strength g becomes smaller correspondingly as shown in Fig. 4(b). We also considered the influences from other parameters including the width/height of the nanowire and the geometry of a triangle. Those parameters can largely affect the g . For example, g will decrease obviously when the distance between two wires is either greater or less than 90 nm (see Fig. S5). In contrast, β is robust to those parameter variations in a certain range (see Fig. S5). Another parameter that can greatly affect the coupling strength g is the transition dipole moment of a QE. The coupling strength g increases proportionally with the transition dipole moment [Fig. 4(c)]. Figures 4(d), 4(e), and 4(f) show the concurrence as a function of time with some of the cases in Figs. 4(a), 4(b), and 4(c), respectively. As expected, the concurrence varies faster with time and reaches a larger maximal value by increasing g and β .

The concurrence time is in picosecond scale. Such a fast period of time is mainly due to the large Ohmic loss in plasmonic nanostructures. On the other hand, this timescale is acceptable and common in the field of ultrafast optical measurement. Regarding the issue of fast decoherence in the pursuit of potential applications in quantum computing, one may consider two solutions. First, the required quantum computing operations can be implemented within the picosecond scale, for example, by accelerating the characteristic time of quantum computation to the femtosecond scale. This may require a well-designed structure just around the QEs or QEs with larger enough transition dipole moments to achieve larger coupling strength g [6–8,17]. The relevant work still requires further efforts. Based on our results, the future designs (like the tips in this work) could possibly not affect the energy transfer efficiency β with the dark plasmon waveguide

here. Second, one may also consider adding a gain medium to effectively compensate the loss in the plasmonic waveguide, thereby significantly increasing the maintenance time of larger entanglement.

IV. CONCLUSION

We analytically consider a general case of the entanglement dynamics between two QEs mediated by a plasmon waveguide. Our results show that both the coupling strength g and the energy transfer efficiency β are crucial for the entanglement magnitude. On the other hand, achieving high values for both g and β simultaneously remains challenging within a common plasmon waveguide system. In light of this, we proposed a dark-gap-plasmon waveguide consisting of two parallel Ag nanowires. Dark plasmon modes can be formed in the gap between the nanowires in such a waveguide, where the leaky (or radiative) feature of propagating plasmon is highly suppressed. This is also reflected by the Q factor of a plasmon mode which is pushed to the material limit. As

a result, the β factor can maintain more than 94% with a distance between QEs over ten operating wavelengths. More results show that β is almost only determined by material loss and is robust to geometry variations of the waveguide. Furthermore, by introducing a tip dimer around each QE in the waveguide, the plasmon-QE coupling strength can reach the strong coupling regime. Our results demonstrate that by engineering dark plasmon, it is possible to simultaneously achieve high coupling strength and energy transfer efficiency for two well-separated QEs. This approach opens the door to the experimental realization of efficient entanglement between two QEs and may hold significant potential for applications in quantum information.

ACKNOWLEDGMENTS

This paper was supported by the National Natural Science Foundation of China (Grant No. 11704416) and the Hunan Provincial Natural Science Foundation of China (Grant No. 2021JJ20076).

-
- [1] R. E. Evans, M. K. Bhaskar, D. D. Sukachev, C. T. Nguyen, A. Sipahigil, M. J. Burek, B. Machielse, G. H. Zhang, A. S. Zibrov, and E. Bielejec, Photon-mediated interactions between quantum emitters in a diamond nanocavity, *Science* **362**, 662 (2018).
- [2] C. R. Kagan, L. C. Bassett, C. B. Murray, and S. M. Thompson, Colloidal quantum dots as platforms for quantum information science, *Chem. Rev.* **121**, 3186 (2020).
- [3] F. J. Garcia-Vidal, C. Ciuti, and T. W. Ebbesen, Manipulating matter by strong coupling to vacuum fields, *Science* **373**, eabd0336 (2021).
- [4] M. Noginov, G. Zhu, A. Belgrave, R. Bakker, V. Shalaev, E. Narimanov, S. Stout, E. Herz, T. Suteewong, and U. Wiesner, Demonstration of a spaser-based nanolaser, *Nature (London)* **460**, 1110 (2009).
- [5] T. W. Ebbesen, Hybrid light-matter states in a molecular and material science perspective, *Acc. Chem. Res.* **49**, 2403 (2016).
- [6] R. Chikkaraddy, B. de Nijs, F. Benz, S. J. Barrow, O. A. Scherman, E. Rosta, A. Demetriadou, P. Fox, O. Hess, and J. J. Baumberg, Single-molecule strong coupling at room temperature in plasmonic nanocavities, *Nature (London)* **535**, 127 (2016).
- [7] K. Santhosh, O. Bitton, L. Chuntonov, and G. Haran, Vacuum Rabi splitting in a plasmonic cavity at the single quantum emitter limit, *Nat. Commun.* **7**, ncomms11823 (2016).
- [8] H. Leng, B. Szychowski, M.-C. Daniel, and M. Pelton, Strong coupling and induced transparency at room temperature with single quantum dots and gap plasmons, *Nat. Commun.* **9**, 4012 (2018).
- [9] R. Liu, Z.-K. Zhou, Y.-C. Yu, T. Zhang, H. Wang, G. Liu, Y. Wei, H. Chen, and X.-H. Wang, Strong light-matter interactions in single open plasmonic nanocavities at the quantum optics limit, *Phys. Rev. Lett.* **118**, 237401 (2017).
- [10] D. G. Baranov, M. Wersall, J. Cuadra, T. J. Antosiewicz, and T. Shegai, Novel nanostructures and materials for strong light-matter interactions, *ACS Photonics* **5**, 24 (2018).
- [11] L. Aolita, F. De Melo, and L. Davidovich, Open-system dynamics of entanglement: A key issues review, *Rep. Prog. Phys.* **78**, 042001 (2015).
- [12] G. Zengin, M. Wersäll, S. Nilsson, T. J. Antosiewicz, M. Käll, and T. Shegai, Realizing strong light-matter interactions between single-nanoparticle plasmons and molecular excitons at ambient conditions, *Phys. Rev. Lett.* **114**, 157401 (2015).
- [13] J. J. Baumberg, J. Aizpurua, M. H. Mikkelsen, and D. R. Smith, Extreme nanophotonics from ultrathin metallic gaps, *Nat. Mater.* **18**, 668 (2019).
- [14] W. Li, R. Liu, J. Li, J. Zhong, Y.-W. Lu, H. Chen, and X.-H. Wang, Highly efficient single-exciton strong coupling with plasmons by lowering critical interaction strength at an exceptional point, *Phys. Rev. Lett.* **130**, 143601 (2023).
- [15] H. Groß, J. M. Hamm, T. Tufarelli, O. Hess, and B. Hecht, Near-field strong coupling of single quantum dots, *Sci. Adv.* **4**, eaar4906 (2018).
- [16] X. Xiong, N. Kongsuwan, Y. Lai, C. E. Png, L. Wu, and O. Hess, Room-temperature plexcitonic strong coupling: Ultrafast dynamics for quantum applications, *Appl. Phys. Lett.* **118**, 2200557 (2021).
- [17] M.-L. Hu, Z.-J. Yang, X.-J. Du, and J. He, Towards strong linear and nonlinear light-matter interactions in hybrid nanostructures of a single molecule and a plasmonic nanocavity, *Phys. Rev. B* **104**, 064311 (2021).
- [18] J. Wolters, J. Kabuss, A. Knorr, and O. Benson, Deterministic and robust entanglement of nitrogen-vacancy centers using low- Q photonic-crystal cavities, *Phys. Rev. A* **89**, 060303(R) (2014).
- [19] B. Casabone, A. Stute, K. Friebe, B. Brandstätter, K. Schüppert, R. Blatt, and T. E. Northup, Heralded entanglement of two ions in an optical cavity, *Phys. Rev. Lett.* **111**, 100505 (2013).
- [20] R. Horodecki, P. Horodecki, M. Horodecki, and K. Horodecki, Quantum entanglement, *Rev. Mod. Phys.* **81**, 865 (2009).
- [21] C. H. Bennett and D. P. DiVincenzo, Quantum information and computation, *Nature (London)* **404**, 247 (2000).
- [22] G. Angelatos and S. Hughes, Entanglement dynamics and Mollow nonuplets between two coupled quantum dots in a

- nanowire photonic-crystal system, *Phys. Rev. A* **91**, 051803(R) (2015).
- [23] M. Hensen, T. Heilpern, S. K. Gray, and W. Pfeiffer, Strong coupling and entanglement of quantum emitters embedded in a nanoantenna-enhanced plasmonic cavity, *ACS Photonics* **5**, 240 (2017).
- [24] M.-T. Cheng, X.-S. Ma, Y.-Q. Luo, P.-Z. Wang, and G.-X. Zhao, Entanglement generation and quantum state transfer between two quantum dot molecules mediated by quantum bus of plasmonic circuits, *Appl. Phys. Lett.* **99**, 223509 (2011).
- [25] M. Otten, R. A. Shah, N. F. Scherer, M. Min, M. Pelton, and S. K. Gray, Entanglement of two, three, or four plasmonically coupled quantum dots, *Phys. Rev. B* **92**, 125432 (2015).
- [26] G.-Y. Chen, N. Lambert, C.-H. Chou, Y.-N. Chen, and F. Nori, Surface plasmons in a metal nanowire coupled to colloidal quantum dots: Scattering properties and quantum entanglement, *Phys. Rev. B* **84**, 045310 (2011).
- [27] K. V. Nerkararyan and S. I. Bozhevolnyi, Entanglement of two qubits mediated by a localized surface plasmon, *Phys. Rev. B* **92**, 045410 (2015).
- [28] V. Karanikolas, Entanglement of quantum emitters interacting through an ultra-thin noble metal nanodisk, *Opt. Express* **28**, 24171 (2020).
- [29] X. Xiong, J.-B. You, P. Bai, C. E. Png, Z.-K. Zhou, and L. Wu, Ultrastrong coupling in single plexcitonic nanocubes, *Nanophotonics* **9**, 257 (2020).
- [30] C. Gonzalez-Ballester, E. Moreno, and F. J. Garcia-Vidal, Generation, manipulation, and detection of two-qubit entanglement in waveguide QED, *Phys. Rev. A* **89**, 042328 (2014).
- [31] W. Pfaff, B. J. Hensen, H. Bernien, S. B. van Dam, M. S. Blok, T. H. Taminiau, M. J. Tiggelman, R. N. Schouten, M. Markham, D. J. Twitchen, and R. Hanson, Unconditional quantum teleportation between distant solid-state quantum bits, *Science* **345**, 532 (2014).
- [32] H. Zheng and H. U. Baranger, Persistent quantum beats and long-distance entanglement from waveguide-mediated interactions, *Phys. Rev. Lett.* **110**, 113601 (2013).
- [33] L. Trifunovic, F. L. Pedrocchi, and D. Loss, Long-distance entanglement of spin qubits via ferromagnet, *Phys. Rev. X* **3**, 041023 (2013).
- [34] W.-K. Mok, D. Aghamalyan, J.-B. You, T. Haug, W. Zhang, C. E. Png, and L.-C. Kwek, Long-distance dissipation-assisted transport of entangled states via a chiral waveguide, *Phys. Rev. Res.* **2**, 013369 (2020).
- [35] L. Ying, M. S. Mattei, B. Liu, S.-Y. Zhu, R. H. Goldsmith, and Z. Yu, Strong and long-range radiative interaction between resonant transitions, *Phys. Rev. Res.* **4**, 013118 (2022).
- [36] J. P. Vasco, D. Gerace, P. S. S. Guimarães, and M. F. Santos, Steady-state entanglement between distant quantum dots in photonic crystal dimers, *Phys. Rev. B* **94**, 165302 (2016).
- [37] J. P. Vasco, P. S. S. Guimaraes, and D. Gerace, Long-distance radiative coupling between quantum dots in photonic crystal dimers, *Phys. Rev. B* **90**, 155436 (2014).
- [38] I. S. Madjarov, J. P. Covey, A. L. Shaw, J. Choi, A. Kale, A. Cooper, H. Pichler, V. Schkolnik, J. R. Williams, and M. Endres, High-fidelity entanglement and detection of alkaline-earth Rydberg atoms, *Nat. Phys.* **16**, 857 (2020).
- [39] Y. Zhang, Y. Tang, Y. Zhou, and X. Ma, Efficient entanglement generation and detection of generalized stabilizer states, *Phys. Rev. A* **103**, 052426 (2021).
- [40] O. Gühne and G. Tóth, Entanglement detection, *Phys. Rep.* **474**, 1 (2009).
- [41] J. M. Raimond, M. Brune, and S. Haroche, *Colloquium: Manipulating quantum entanglement with atoms and photons in a cavity*, *Rev. Mod. Phys.* **73**, 565 (2001).
- [42] A. Gonzalez-Tudela, D. Martín-Cano, E. Moreno, L. Martín-Moreno, C. Tejedor, and F. J. Garcia-Vidal, Entanglement of two qubits mediated by one-dimensional plasmonic waveguides, *Phys. Rev. Lett.* **106**, 020501 (2011).
- [43] Y. Li, A. Nemilentsau, and C. Argyropoulos, Resonance energy transfer and quantum entanglement mediated by epsilon-near-zero and other plasmonic waveguide systems, *Nanoscale* **11**, 14635 (2019).
- [44] S. A. H. Gangaraj, A. Nemilentsau, G. W. Hanson, and S. Hughes, Transient and steady-state entanglement mediated by three-dimensional plasmonic waveguides, *Opt. Express* **23**, 22330 (2015).
- [45] J.-S. Ryom, N.-C. Kim, M.-C. Ko, and S.-I. Choe, Entanglement of two quantum dots with azimuthal angle difference in plasmonic waveguide system, *Plasmonics* **17**, 949 (2022).
- [46] C. E. Susa, J. H. Reina, and R. Hildner, Plasmon-assisted quantum control of distant emitters, *Phys. Lett. A* **378**, 2371 (2014).
- [47] J. Liu, G. Chen, L. Li, R. Liu, W. Li, G. Liu, F. Wu, and Y. Chen, Radiative coupling of two quantum emitters in arbitrary metallic nanostructures, *Sci. Rep.* **12**, 6901 (2022).
- [48] D. Dzsojtan, A. S. Sørensen, and M. Fleischhauer, Quantum emitters coupled to surface plasmons of a nanowire: A Green's function approach, *Phys. Rev. B* **82**, 075427 (2010).
- [49] D. Martín-Cano, A. Gonzalez-Tudela, L. Martín-Moreno, F. J. Garcia-Vidal, C. Tejedor, and E. Moreno, Dissipation-driven generation of two-qubit entanglement mediated by plasmonic waveguides, *Phys. Rev. B* **84**, 235306 (2011).
- [50] D. Martín-Cano, L. Martín-Moreno, F. J. García-Vidal, and E. Moreno, Resonance energy transfer and superradiance mediated by plasmonic nanowaveguides, *Nano Lett.* **10**, 3129 (2010).
- [51] H. Walther, B. T. Varcoe, B.-G. Englert, and T. Becker, Cavity quantum electrodynamics, *Rep. Prog. Phys.* **69**, 1325 (2006).
- [52] P. Törmä and W. L. Barnes, Strong coupling between surface plasmon polaritons and emitters: A review, *Rep. Prog. Phys.* **78**, 013901 (2014).
- [53] E. Waks and D. Sridharan, Cavity QED treatment of interactions between a metal nanoparticle and a dipole emitter, *Phys. Rev. A* **82**, 043845 (2010).
- [54] See Supplemental Material at <http://link.aps.org/supplemental/10.1103/PhysRevB.110.075432> for derivations of entanglement between QEs, numerical method, and additional results of Figs. S1–S5.
- [55] W. K. Wootters, Entanglement of formation of an arbitrary state of two qubits, *Phys. Rev. Lett.* **80**, 2245 (1998).
- [56] T. Hümmer, F. J. Garcia-Vidal, L. Martín-Moreno, and D. Zueco, Weak and strong coupling regimes in plasmonic QED, *Phys. Rev. B* **87**, 115419 (2013).
- [57] T. V. Shahbazyan, Spontaneous decay of a quantum emitter near a plasmonic nanostructure, *Phys. Rev. B* **98**, 115401 (2018).
- [58] M. Pelton, Modified spontaneous emission in nanophotonic structures, *Nat. Photonics* **9**, 427 (2015).

- [59] R. A. Shah, N. F. Scherer, M. Pelton, and S. K. Gray, Ultrafast reversal of a Fano resonance in a plasmon-exciton system, *Phys. Rev. B* **88**, 075411 (2013).
- [60] F. Wang and Y. R. Shen, General properties of local plasmons in metal nanostructures, *Phys. Rev. Lett.* **97**, 206806 (2006).
- [61] X.-T. Tang, L. Ma, Y. You, X.-J. Du, H. Qiu, X.-H. Guan, J. He, and Z.-J. Yang, Relations between near-field enhancements and Purcell factors in hybrid nanostructures of plasmonic antennas and dielectric cavities, *Opt. Express* **32**, 16746 (2024).